Unlocking the performance of wet and dry-fractionated pea proteins in 3D food printing

Future Foods 14 (2026) 101128

Contents lists available at ScienceDirect

Future Foods

journal homepage: www.elsevier.com/locate/fufo

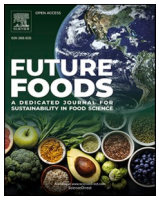

Unlocking the performance of wet and dry-fractionated pea proteins in 3D food printing

Isabel Badager [a], Annika Krona [b], Mehdi Abdollahi [a,*]

[a] Department of Life Sciences-Food and Nutrition Science, Chalmers University of Technology, Kemigården 4, Gothenburg, SE-41296, Sweden
[b] RISE Research Institutes of Sweden, Agriculture and Food, Box 5401, 402 29, Gothenburg, Sweden

ARTICLE INFO

Keywords:
3D food printing
Pea protein
Plant-based protein
Protein fractionation method
Hydrocolloids

ABSTRACT

This study investigated how fractionation method (dry fractionated (PPC) vs. wet fractionated (PPI)) affects pea protein 3D printability and rheological behavior at 10–50 wt.%. The potential of preheating and hydrocolloid addition (carrageenan, pectin, and xanthan gum) in enhancing their 3D printability, texture and microstructure was also evaluated. PPI alone showed good printability at 30 wt.%, while PPC remained unprintable even at 50 wt.% due to fiber-induced network disruption and low viscosity. However, PPC's printability was restored at 40 wt.% through preheating and hydrocolloid addition. PPC and PPI responded very differently to hydrocolloids: pectin improved 3D printing resolution for PPI but weakened post-steaming texture, while in PPC, only pectin provided printability without adversely affecting texture. Overall, PPI demonstrated inherent 3D printability while PPC required modification to achieve comparable performance. Hydrocolloid functionality was protein-type specific, and successful 3D printing of pea protein requires tailored formulation strategies depending on the fractionation method.

1. Introduction

3D food printing by extrusion is a promising technology for structuring plant-based proteins into customized and complex shapes, offering flexibility in design, nutritional tailoring, and ingredient composition. This is particularly attractive for meat analogue development, where structure, texture, and functionality must be carefully engineered. Compared to conventional processes like high-moisture extrusion, 3D printing operates at lower pressures and temperatures (Wen et al., 2022), offering advantages in energy use and potential preservation of functional ingredients. A critical factor in successful 3D printing of plant-based protein is the printability - its ability to flow through a nozzle (extrudability) and maintain its shape after deposition (buildability) (Wilms et al., 2021). These properties are largely governed by the rheological behavior of the protein, which is driven by its source, extraction method, purity, and concentration and can be tuned through formulation strategies (Wilms et al., 2021).

Two primary industrial routes for concentrating plant proteins are dry and wet fractionation which yield two distinct protein ingredients: protein concentrate and protein isolate. Protein isolates are normally associated with higher protein purity (>80 % protein) and price, while also requiring more resource-demanding processing that results in significant protein denaturation compared to protein concentrates (~50-60% protein) (Schutyser et al., 2015; Sajib et al., 2023). Due to their milder processing, dry fractionated protein concentrates retain more impurities such as fibers, fats, minerals and polysaccharides (Boukid et al., 2021). These are components that might later be reintroduced in 3D printing formulations, making their initial removal unnecessary. It is, for example, common to add hydrocolloids, including starch, to improve the printability of food proteins that naturally exist in protein concentrates. On the other hand, these impurities might negatively affect the taste and nutritional value as well as on the printability when aiming for high-protein products or specific rheological properties. Previous studies suggest that less refined and minimally denatured dry fractionated protein concentrates are good enough for meat analogues, especially when using extrusion technology (De Angelis et al., 2023, Schutyser et al., 2015) and sometimes offer better protein functionality and product quality (Pelgrom et al., 2013, Lie-Piang et al., 2023). However, it remains unclear whether the performance of these two ingredients translates similarly in the context of 3D food printing, which relies on different flow and solidification mechanisms compared to thermomechanical processing.

* Corresponding author.
E-mail address: khozaghi@chalmers.se (M. Abdollahi).

https://doi.org/10.1016/j.fufo.2026.101128
Received 23 November 2025; Received in revised form 27 June 2026; Accepted 14 July 2026
Available online 15 July 2026

Furthermore, formulation parameters such as ingredient concentration, thermal pre-treatment, and hydrocolloid addition can significantly influence the printability of protein-based inks. Hydrocolloids like pectin, xanthan gum, and carrageenan are commonly used to enhance viscoelasticity, improve interlayer adhesion, and reinforce network formation, though their effectiveness may vary depending on the protein source and its degree of purity. Despite growing interest in using less refined, dry-fractionated protein concentrates in 3D food printing, there is still limited understanding of how their inherently retained polysaccharides and other non-protein components influence printability, especially compared with high-purity protein isolates. These compositional differences may affect not only the base printability of each protein system but also the type and extent of formulation modifications required (e.g., through hydrocolloids or heat treatments) to achieve optimal printing performance. Moreover, how these intrinsic (e.g., protein concentration) and extrinsic (e.g., preheating, hydrocolloid addition) factors affect the printability and the final quality of printed products from a protein concentrate and isolate in a side-by-side comparison remains underexplored.

Therefore, this study was aimed to systematically investigate the 3D printability of pea protein concentrate (PPC) and pea protein isolate (PPI) and to examine which ingredient is inherently more suitable for extrusion-based 3D food printing and whether their limitations can be mitigated. Specifically, our objectives were to (i) understand how the type of protein ingredient and concentration (10-50%w) as key intrinsic factors affect their rheological properties and 3D printability; (ii) asses the effect of different extrinsic factors, including preheating and hydrocolloids additives (carrageenan, pectin and xanthan gum), on improving the rheological properties and the printability of PPI and PPC; and finally (iii) investigate how these factors influence the textural, rheological and microstructural properties and water mobility of the 3D printed objects produced from each protein ingredient.

2. Material and methods

2.1. Materials

Commercial pea protein isolate Nutralys® F85M (protein content = 80.87±0.31%, N=6.25) was acquired from Roquette (Roquette, France) produced via wet fractionation and pea protein concentrate (Vestkorn A/S, Denmark), contained around 90 %-93 % dry matter, 54 %-56 % protein, 15 %-20 % carbohydrates, 15 %-17 % dietary fiber, 3%-5% total fat, and 5.5 %-6.5 % ash which was produced through dry fractionation. The hydrocolloids used were pectin from apple (Fluka, 70-75% esterification), xanthan gum (Sigma-Aldrich), and carrageenan (Sigma-Aldrich, Cas: 9000-07-1).

2.2. Preparation of printing ink from pea protein ingredients

2.2.1. Effect of protein ingredient concentration

To evaluate the effect of protein concentration on the properties of the printing ink, PPI and PPC were each individually mixed with distilled water at various concentrations. PPC was prepared at concentrations of 10, 20, 30, 40, and 50 wt.%, while PPI was prepared at 10, 20, 30 wt.%. Based on pretests, PPI concentrations of 40 wt.% or higher were excluded from further testing as they produced a grainy and crumbly texture unsuitable for printing. The samples were hydrated and mixed in a closed electric chopper intermittently for 5-15 seconds for one hour at room temperature until the samples were visibly homogeneous. For the powder to be equally hydrated, the PPI samples were mixed quickly and thoroughly in the beginning to avoid graininess and mixed less at the end. The PPC samples were mixed moderately over the entire hour for the samples to be evenly hydrated. After preparation, all samples were stored overnight at 4°C and then equilibrated for one hour at room temperature before the trials.

To investigate the effect of preheating prior to filling the cartridge, the samples were also heated in a 60°C water bath in 50 ml falcon tubes (in plastic bags) for 20 min and left to cool down at room temperature for 90 min before being used. These samples are denoted with an *h* at the end when representing the results.

2.2.2. Effect of hydrocolloid addition

For the second trial, printing inks were prepared using 40 wt.% and 30 wt.% of PPC and PPI, respectively, were mixed with hydrocolloids, specifically pectin (*Pec*), xanthan gum (*Xan*), and carrageenan (*Carr*) at a concentration of 1.5 wt.% prior to adding distilled water. Then the sample preparation continued as described in section 2.2.1 and used immediately for 3D printing. Pretests of addition of pectin to PPI at 20 and 30 w % showed that PPI at 30 wt.% had a larger potential as printing ink.

2.3. Rheological analysis of the 3D printing inks

Viscoelastic properties of all inks were analyzed using a dynamic rheometer (Paar Physica Rheometer MCR 300, Anton Paar GmbH, Austria) equipped with a serrated probe (PP25/P2) and a serrated plate (TEK-150) with a gap setting of 1 mm. After loading, the samples were covered with mineral oil, and a moisture trap and a waterlock were used. Prior to analysis, there was a two-minute resting period. For the trial on the effect of addition of a hydrocolloid with preheating, the samples were preheated on the rheometer at 60°C for 20 min prior to the analysis. All the measurements were done with 2 or 3 replicates except for the frequency sweep for PPC10 which had no replicates.

2.3.1. Oscillatory amplitude sweep

An oscillatory amplitude sweep was performed to find the linear viscoelastic (LVE) region and flow point for the pea protein-based inks. The strain was varied between 0.01 to 1000 (%) (6Pt./dec), using an angular frequency of 10 rad/s at a temperature of 25°C (Abdollahi et al., 2025). For the trial on the addition of a hydrocolloid together with preheating, the temperature was kept constant at 60°C to simulate the heating in the cartridge. The difference between the storage modulus (G') and loss modulus (G") was used to get an insight into the viscoelasticity of a sample (Joyner, 2019). The flow point, the point at which the shear stress is high enough to make the sample start to flow (Maldonado-Rosas et al., 2022; Outrequin et al., 2023), was obtained from the intersection between the elastic modulus and viscous modulus.

2.3.2. Rotational viscosity flow curve measurement

The flow curve measurement of the protein inks was conducted to examine their shear-thinning behavior. Shear viscosity was measured by varying the shear rate logarithmically from 0.001 to 100 (1/s) at 25°C under rotation mode. For the trial on the addition of a hydrocolloid together with preheating, the temperature was kept constant at 60°C.

The model used to describe the fluids' shear thinning behavior was the Carreau-Yasuda model as seen in Equation 1, which describes the viscosity (η) as a function of the shear rate ($\dot{\gamma}$) (Osswald & Rudolph, 2015):

$$\eta = \frac{\eta_0}{(1 + (\lambda * \dot{\gamma})^a)^{(1-n)/a}} \quad (1)$$

where η_0 is the zero shear viscosity, λ is the relaxation time, n is the power law index, and a is a regression parameter.

2.3.3. Frequency sweep measurement

Change in the viscoelastic properties of the inks in response to variation of frequency between 200 and 0.1 rad/s at 25°C was measured in LVR of the samples using a strain of 0.05 and under oscillation mode. For the trial on the addition of hydrocolloid with preheating, the temperature was kept constant at 60°C.

2.3.4. Three interval thixotropy test

The recovery of the samples' viscosity after 3D printing was evaluated using a three-interval thixotropy test (3ITT) by applying a high shear strain for a period to mimic the printing conditions during extrusion (Johansson et al., 2025). After shearing, the viscosity at-rest represents the post-extrusion condition on the printing platform. The post-shearing viscosity was compared to the recorded viscosity of the sample before increasing the shear strain to evaluate its recovery, as performed by Maldonado-Rosas et al. (2022). In the initial stage of the 3ITT, the sample was held for 200 s at a shear strain of 0.05 %, representing the sample resting in the printing syringe, followed by an increase to 10 % for 100 s, followed by a 200 s period of a shear strain of 0.05 % at an angular frequency of 10 rad/s. For the trial on the addition of hydrocolloids with preheating, the temperature was kept constant at 60°C, to mimic the heating in the cartridge, until the last interval at which it was set to 25°C, to mimic the room temperature at the printing plate, and the last interval was extended to 300 s.

2.3.5. Tack-adhesion test

The tack-adhesion test was performed using a single-cycle uniaxial tensile program with a texture analyzer (Perten TVT 6700, Perten Instruments, Australia), using a flat compression plate ∅ = 40 mm compression plate and a 10 kg load cell (Perten Instruments, 672040, Australia). The pea protein samples were loaded on the measuring plate and an initial gap distance of 3 mm was set. Then, the probe was raised at a speed of 0.5 mm/s and manually stopped once the sample separated into two. The peak force was recorded (n=3, 4 or 5) and the length at breakage (n=3 or 4) was measured with a caliper. For all samples except PPI30 and PPI30Carr, a trigger force of 1 g was used. For PPI30 and PPI30Carr the trigger force was increased to 2500 g, however no peak force could be recorded for these samples.

2.4. 3D printing and evaluation of the printed objects

For pea protein samples with low viscosity (PPC40h, PPI20, PPI20h, and PPC40Carr), the printing cartridge (a 60 ml stainless steel syringe) was filled by directly pouring the material into it. For the stickier protein samples (PPC50, PPC50h, PPC40Xan and PPC40Pec), a modified syringe-like tool with an open barrel bottom was used to facilitate filling. After filling the cartridge, the bottom was slammed to remove excess air.

3D models for two objects, a square (hollow) and a cube (filled in), were transformed into gcode files for printing using a GcodeCreator. The objects were printed using Procusini 5.0 Food Printer (Procusini, Germany) with a single moving cartridge with a diameter of 27 mm equipped with ∅ = 1.0 mm nozzle. The square and the cube had a height of 15 mm and 10 mm, respectively, with a side length of 20 × 20 mm printed with a layer height of 0.5 mm, and a track width of 1.0 mm. The print speed was set at 600 mm/min, the moving speed at 700 mm/min, and the extrusion multiplier was 1.5. The extrusion and retraction speed were 8000 mm/min.

The printing inks that dripped from the cartridge were considered unprintable. To evaluate the effect of PPI and PPC at varying concentrations, only the square object was printed. For the samples containing hydrocolloids, both square and cube objects were printed.

2.4.1. Post-processing of the printed objects by steaming

To investigate whether the 3D printed object was able to withstand post-processing, the 3D printed cubes of the pea samples with hydrocolloids and PPI30 as a control were steamed for 5 min with Cuisinart (STM1000E). The temperature was aimed to be between 80 and 85°C, and it was kept no lower than 70 and no higher than 90°C. The temperature in the steamer was measured with a thermometer and regulated to keep it in the range.

2.4.2. Uniaxial compression test of the post-processed printed objects

A compression test was performed on the post-processed cubes (n=3 or 4) with a single cycle compression of 30 % with a ∅ = 40 mm compression plate (Perten Instruments, 672040), using a 10 kg load cell of a texture analyzer (Perten TVT 6700, Perten Instruments, Australia). An initial speed of 3 mm/s was used with a test speed and retraction speed of 1mm/s and a trigger force of 10 g.

2.5. Confocal laser scanning microscopy (CLSM)

To evaluate how the polysaccharides affected the protein structuring in formed gels, samples were prepared in the same way as described in section 2.2.2, where PPI at 30 wt.% and PPC at 40 wt.% were gelled with and without the hydrocolloids as described by Sajib et al. (2023) with slight modifications. The samples were filled into 10 ml syringes which were heated at 85°C for 20 min in a water bath and then put on ice water before being stored overnight at 4°C. The gel samples were placed on a drop of staining solution on a cover slide. Proteins were stained with Texas red (shown in red) and fibers with direct yellow 96 (shown in green). Samples were examined with an inverted confocal laser scanning microscope (Leica TCS SP5, Heidelberg, Germany) using a HCX PL APO CS 63.0 × 1.20 WATER UV objective. A 488 nm argon laser and a 594 nm HeNe laser were used for excitation and emission were collected at 502-531 nm and 610-649nm. Micrographs were captured with 1024 × 1024 pixels, eight line averages.

2.6. Water distribution analysis by low-field nuclear magnetic resonance

To determine the water distribution in the samples, the transverse relaxation time (T2) was measured in the gels (n=2) with time domain low-field nuclear magnetic resonance spectroscopy (LF-NMR) using Bruker minispec mq20 (NMR MiniSpec mq20, Bruker, Germany) equipped with a 10 mm probe. The measurements were performed at 20°C in real detection mode using the Carr-Purcell-Meiboom-Gill pulse sequence. The number of scans was 44, the recycle delay 2.5 s, using 0 dummy slots. The bandwidth was 20,000 kHz, using a 0.1 tau pulse separation between 90° to 180°, and the 90° and 180° pulse lengths were 2.76 μs and 5.54 μs, respectively. The number of data points for fitting was 3000 and the number of not fitted echoes was 1. To obtain the relaxation peaks, the data were processed using CONTIN (Provencher, 1982).

2.7. Statistical analysis

The statistical analysis and plotting of rheological and textural analysis data were performed in MATLAB R2023b. For all replicates, the mean and standard deviation were calculated. For the viscosity flow curve, Carreau-Yasuda data fitting was performed in the software Rheoplus/32, version V3.40. The plotting of TD-NMR relaxation peaks, the integration, and statistical analysis were performed in OriginPro 2023. To determine statistical significance, one-way ANOVA was performed followed by Tukey's test using a significance level of $\alpha = 0.05$ was performed, and the flow points and zero shear viscosities were log-transformed (base-10) before the statistical analysis.

3. Results and discussion

3.1. Effect of concentration of PPI and PPC

3.1.1. Rheological properties

The rheological results of PPC at 10, 20, and 30 wt.% and PPI at 10 wt.%, with and without heating, can be found in **Supplementary A in Fig. A.1.** As shown by their low viscosities, these samples were very fluid and unable to support their own weight in the syringe and flowing without applying any force. This behavior indicates insufficient intermolecular interactions or network formation at these concentrations, which are critical for maintaining shape fidelity during extrusion-based 3D printing. As a result, these formulations were deemed unsuitable for

printing and were not included in further analyses.

The shear stress amplitude sweep is an effective tool for determining the flow points of viscoelastic materials, providing insight into their supportability and buildability as 3D printing inks (Liu et al., 2018; Maldonado-Rosas et al., 2022). The flow points of PPI20, PPC40, and PPC50 were relatively low at approximately 60 Pa and 40 Pa, respectively. In contrast, PPI30 exhibited a significantly higher flow point of around 4500 Pa (see Fig. B.1 and Table B.1 in Supplementary B), suggesting significantly greater resistance to deformation under stress. This implies that PPI30 possesses superior buildability and is more capable of supporting successive printed layers without collapsing. The large increase in flow point from PPI20 to PPI30 indicates a threshold concentration at which a continuous protein network begins to form, leading to a dramatic enhancement in mechanical strength. In contrast, the limited increase in flow point with increasing PPC concentration suggests that PPC does not form an effective network structure within the tested range, which is essential for improving viscosity and structural integrity (Ainis et al., 2023). Notably, PPI30 also exhibited much higher storage (G') and loss (G") moduli compared to the other samples (see Fig. 1a), indicating a stronger and more elastic network, despite having a higher

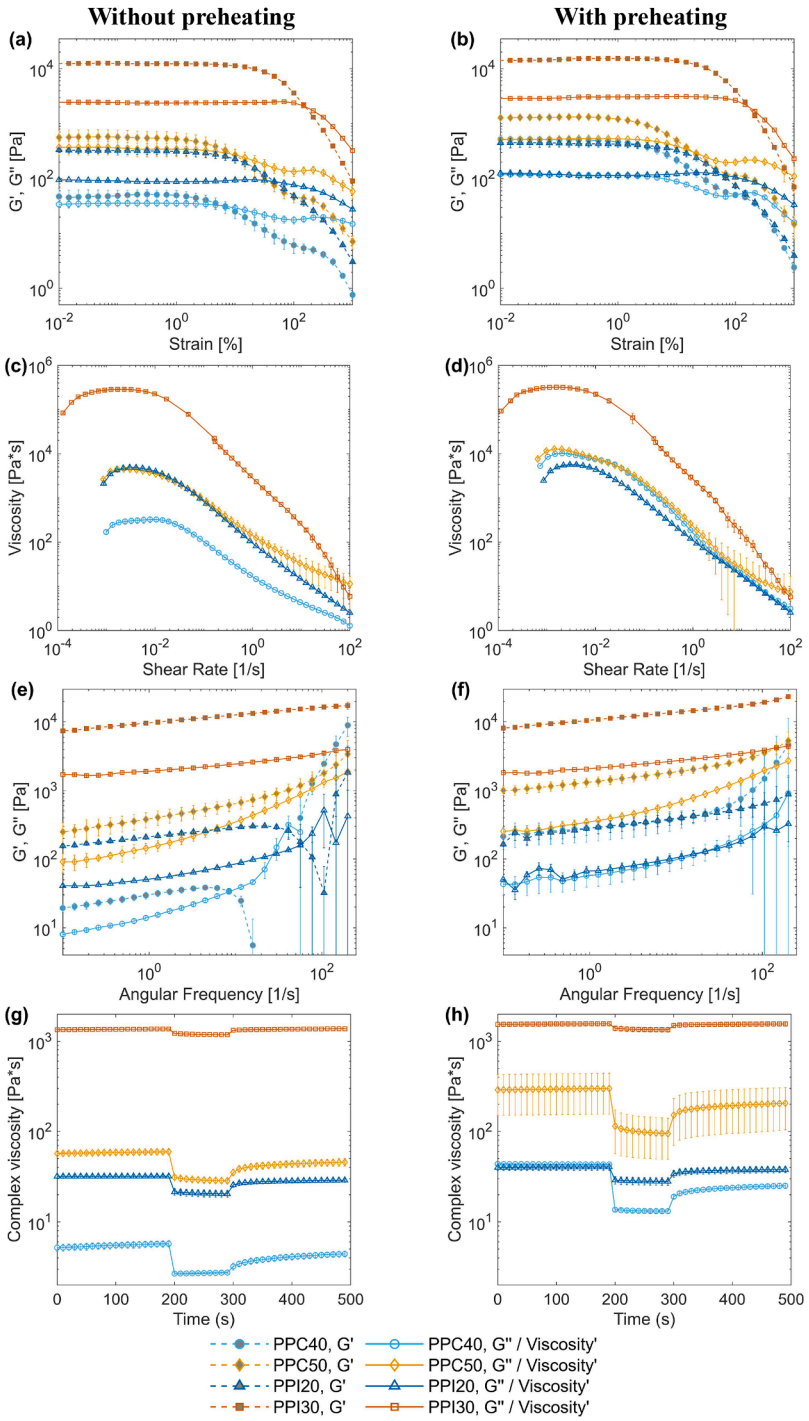

Fig. 1. Rheological properties, effect of concentrations: (a,b) oscillatory amplitude sweep, (c,d) viscosity flow curve, (e,f) frequency sweep, (g,h) three interval thixotropy test during low (0.05 %) and high (10 %) shear strain. Pea protein concentrate, PPC40 and PPC50 at 40 and 50 wt.% respectively, and pea protein isolate, PPI20 and PPI30 at 20 and 30 wt.% respectively without preheating (a,c,e,g) and with preheating (b,d,f,h) at 60°C before filling the cartridge.

water content than PPC50. This highlights the role of protein concentration and structure-forming ability in determining rheological properties relevant to 3D printing performance. PPI30 showed a slight increase in flow point and G' and G" with preheating (see Fig. 1b). This suggests that thermal treatment promotes partial protein unfolding, enhancing intermolecular interactions such as hydrogen bonding or hydrophobic associations, which contribute to network strengthening. This is in alignment with what Chen et al. (2022) found-that heating of soy protein isolate to some extent increased the flow point, and that the heating also improved the stability of the 3D printed object.

Shear-thinning behavior is desirable in extrusion-based 3D printing, as the material should stay in the cartridge when no force is applied, indicated by their zero shear viscosity, start to flow once pressure is applied and lastly be stable once it is at rest after being printed (Tan et al., 2018; Zhang et al., 2015). The viscosity flow curve can also indicate how strong the shear-thinning property of a material is (Zhang et al., 2015). All samples exhibited shear thinning behavior, as seen in Fig. 1c and Fig. 1d. Among the samples, PPI30 showed the strongest shear thinning behavior as it had the steepest descent of the curve. It also had a significantly higher zero shear viscosity (about 170 kPa·S) compared to the other samples which were about 3.6, 3.8, and 0.27 kPa·S for PPI20, PPC50 and PPC40, respectively. This suggests that PPI30 forms a more robust internal network capable of resisting flow at low shear, which is beneficial for maintaining shape fidelity during printing. Preheating increased the viscosity of PPC samples regardless of protein concentration, with zero shear viscosity increasing significantly to approximately 7.9 and 10 kPa·s for PPC40 and PPC50, respectively (Table A.1 in Supplementary A). In contrast, the effect of preheating on PPI was less pronounced, increasing the zero shear viscosity insignificantly to about 190 kPa·s for PPI30 and 4.1 kPa·s for PPI20. This indicates that PPC is more responsive to thermal treatment, likely due to increased molecular mobility or partial denaturation that facilitates new interactions during heating which can be attributed to PPCs lower purity and more complex composition. Unlike PPI, which is highly purified and predominantly composed of protein, PPC contains residual non-protein components such as fibers, starches, and other soluble polysaccharides. Upon heating, these components can undergo thermal swelling, gelatinization (in the case of starch), and interactions with proteins, contributing to increased viscosity and network formation. Starch, in particular, can gelatinize and entrap water, while fibers may physically entangle with proteins or form particulate networks, both of which enhance the bulk viscoelasticity. As a result, preheating may have a greater impact on the rheological behavior and printability of PPC formulations compared to PPI.

PPI30 had a constantly higher G' than G" in the frequency sweep (see Fig. 1e), indicating solid-like behavior (Joyner, 2019) and a stable gel network. Preheating at 60°C had minimal impact on this viscoelastic profile (Fig. 1f), suggesting that PPI30's network is already well-established at room temperature and not significantly altered by mild thermal treatment. This aligns with the previous amplitude sweep results showing a high flow point and with the strong shear-thinning and zero shear viscosity observed in PPI30, all pointing toward a robust, concentration-dependent protein network that supports shape fidelity under shear and post-printing. For PPC50, G' was also constantly higher than G", although both changed notably with the frequency, implying that it had a soft gel structure. The preheating of PPC50 resulted in an increased gap between the G' and G", and both decreased at lower angular frequencies, indicating thermal enhancement of gel strength but also some relaxation behavior typical of soft gels (Joyner, 2019). These results are consistent with the shear tests, where PPC showed a notable increase in zero shear viscosity after heating, likely due to starch gelatinization and polysaccharide–protein interactions. PPI20 and PPC40 had a crossover between the G' and G", indicating lower viscoelasticity and, therefore, having more liquid-like properties. This behavior can predict poor printability and buildability, as softer, less elastic pastes cannot maintain shape integrity during extrusion and post-printing.

The 3-Interval Thixotropy Test (3ITT) further highlights the differences in structural integrity and recovery behavior among the samples. As shown in Fig. 1g and Fig. 1h, PPI30 and its preheated counterpart (PPI30h) exhibited substantially higher complex viscosities than the other samples throughout the test, indicating a more cohesive and resilient internal network. This observation is consistent with previous findings from the amplitude and frequency sweeps, where PPI30 displayed high flow point, low frequency dependence, and solid-like viscoelastic behavior, all of which are desirable for extrusion-based 3D printing. In contrast, PPC50 showed a greater drop in complex viscosity during the high-shear interval compared to PPI20, and also demonstrated poorer recovery during the final resting period. This suggests that PPC50 is more susceptible to structural breakdown under shear and has a slower or incomplete rebuilding of its network after deformation. A rapid and sufficient recovery is essential for supporting the next printed layer during additive manufacturing (Liu et al., 2019), and these results point to a potential limitation of PPC in terms of post-extrusion supportability. This indicates that during printing, PPC might not recover as well after being subjected to a force. For the 3ITT, the shear strain in the first and last interval should be within the LVE region, and in the second interval, it should be outside of the LVE region (Toker et al., 2015). The strain of 0.05 % which was used in the low strain regions in the 3ITT was within the LVE region for all samples, including the preheated ones. The higher strain of 10 % in the 3ITT was, however, not clearly outside of the LVE region for PPI30 and PPI30h. This might mean that the internal breakage might not be as high for PPI30 during extrusion. Interestingly, after preheating, PPI20h and PPC40h initially showed similar complex viscosities. Yet, PPC40h experienced a sharper viscosity drop under high strain and recovered less during the final interval. One possible explanation is that the applied strain exceeded the LVE region more significantly for PPC40h than for PPI20h, resulting in more extensive internal network breakdown. Regardless of the specific mechanism, the lower recovery of PPC40h underlines its limited ability to restore structure post-shear, which would negatively impact print quality and layer stability.

In general, PPI exhibited stronger gel-like and solid-like properties than PPC, which is particularly seen in the behavior of PPI30, which despite its lower dry matter content had a significantly higher flow point (4500 Pa) compared to PPC50 (around 40 Pa). This indicates that PPI-based pastes can withstand a greater force before flowing, contributing to which could contribute to greater supportability and buildability for 3D printing applications (Liu et al., 2019). Additionally, PPI30 demonstrated a more pronounced shear-thinning behavior than the PPC samples, which could help in achieving smooth printing and during extrusion, and a higher zero shear viscosity which could result in greater stability post-printing. The G' and G" values indicated more solid-like behavior for PPI, especially at 30 wt.%, compared to PPC even at a very high concentration (50 wt.%). Frequency sweep tests showed that while PPC still exhibited a weak gel structure, it had higher frequency dependence and a softer, more deformable consistency than PPI, indicating less robust network formation. This was also reflected in 3ITT recovery behavior, where PPC exhibited lower structural recovery after shearing, suggesting limitations in its ability to maintain shape in layer-by-layer deposition.

Overall, the inferior performance of PPC could not be compensated for by simply increasing concentration, suggesting that differences in rheological performance are not solely a function of dry matter or protein content. Instead, they are strongly influenced by the presence of non-protein components in PPC—such as starch and fiber—which likely interfere with protein–protein interactions and the formation of a cohesive viscoelastic network. Preheating partially improved the viscoelastic and recovery properties of PPC, likely due to enhanced protein unfolding and interaction potential, but it did not close the gap compared to PPI.

3.1.2. 3D printability of PPI and PPC without and with preheating

The visual appearance of the 3D printed squares of PPC and PPI without and with preheating can be seen in Fig. 2. The only printable sample of PPC was PPC50, which still had low self-supportability and buildability. Both PPI20 and PPI30 were extrudable, although PPI30 was the only printed object from the tested concentrations which retained the designed shape and had a good buildability, although it still had some hanging and cracked lines. The preheating of PPI at 60°C before filling the cartridge only affected the 3D printability marginally. Previously, Chen et al. (2022) have demonstrated that heating to some extent can improve the stability of printed soy protein isolate. However, PPI30 appeared to have a slightly worse printing resolution after the preheating, with more hanging and cracked lines. The difference might be that PPI30 had a stronger structure from the start compared to the soy protein isolate in the study of Chen et al. (2022), meaning that there was little room to improve while PPI20 was very loose. The effect of heating on PPI might therefore have been better seen in an object with a concentration between 20 and 30 wt.%. Preheating had a stronger effect on the printability of PPC, where it slightly increased the buildability of PPC50 and improved the resolution as seen by the clearly distinguishable lines, although it still had low self-supportability and did not respond properly to the retraction of the piston resulting in a loop. This slightly improved 3D printability of PPC50 by heating might partially be explained by the increase in zero shear viscosity caused by heating, as well as the increased flow point, and partially by the more gel-like behavior that was seen in the frequency sweep. The heat treatment of PPC40 resulted in it being extrudable although it had poor buildability and standability. PPC40h and PPI20h showed similar, poor printability although PPC40h flowed out more, which could be due to PPI20h recovering better after being printed, as seen in the 3ITT (see Fig. 1h).

Both PPI30 and PPC50 had relatively high protein content, comparable to meat which contains around 20-21 % protein (Coultate, 2016), which is ideal when creating a meat analogue. In this study, PPI at 20 wt.% had poor printability with no buildability. Previously, Ainis et al. (2023) were able to print pea protein isolate (Nutralys® F85M) at 19 and 21 wt.% with water and a pH 7.0 buffer (50 mM MOPS, 3-(N-morpholino)-propanesulfonic acid). The pH of PPI20 was measured to 7.4, which unlikely explains the entire difference in printability. Therefore, the discrepancy in printability remains unexplained, although it might be due to several factors such as batch effects and storing conditions.

Connecting the printability of the protein ingredients to their rheology, PPI30 had a high zero shear viscosity in the flow curve and a gel-like structure in the frequency sweep. This might mean that a zero shear viscosity of somewhere around the magnitude of 100 kPa·s, such as the one PPI30, is necessary for 3D printing of pea protein-based inks. Despite having similar protein concentrations (about 24.3 and 25.4 % protein, respectively), PPI30 and PPC50 had markedly different rheological properties and printability, with PPI30 having good printability and PPC50 having poor buildability. The difference in 3D printability and rheological properties of PPC and PPI could be related to the higher level of non-protein components in PPC such as starch, fibers, and sugars possibly interfering with the protein-protein interactions and structure formation. Venkatachalam et al. (2023) found that a larger addition of fiber to a formula consisting of different amounts of protein, starch, and fibers resulted in both a lower flow point and a lower necessary force to extrude the material. The difference in protein network could also be attributed to the state of the proteins, since commercial protein isolates tend to be denatured while the concentrate has more native proteins (Dumoulin et al., 2021). It has previously been shown that gel-forming ability and rheological properties of PPI improved by an increase in protein denaturation induced by using high pH and temperature during the protein isolation (Sajib et al, 2023).

The zero shear viscosity and flow point alone might however not be completely indicative of the printing performance. Rather it is likely, that a combination of rheological properties such as zero shear viscosity, viscoelasticity and the flow point describes the printability. One example of this is that despite its poor printability, PPC50h performed slightly better in buildability and supportability than PPI20h. Previously, the supportability has been linked to a higher flow point (Maldonado-Rosas et al., 2022). However, the flow points of PPI20h and PPC50h were close and insignificantly different (around 100 and 80 Pa, respectively, see Table B.1 in supplementary B), and the difference in printability can therefore not be explained by the flow point. PPC50h's better buildability might, however, be explained by the difference in zero shear viscosity between the samples (PPC50h around 10 kPa·s and PPI20h around 4 kPa·s) and that PPC50h showed a higher viscoelasticity in the frequency sweep. An example of that the zero shear viscosity might not be completely indicative of the printability is that a PPC40h flowed out more compared to PPI20h although PPC40h had an insignificantly higher zero shear viscosity (about 8 kPa·s compared to 4 kPa·s for PPI20h). The rheological properties of PPC40h and PPI20h were otherwise similar, with the main difference that PPC40h had a lower recovery in the 3ITT. This difference in recovery might account for why

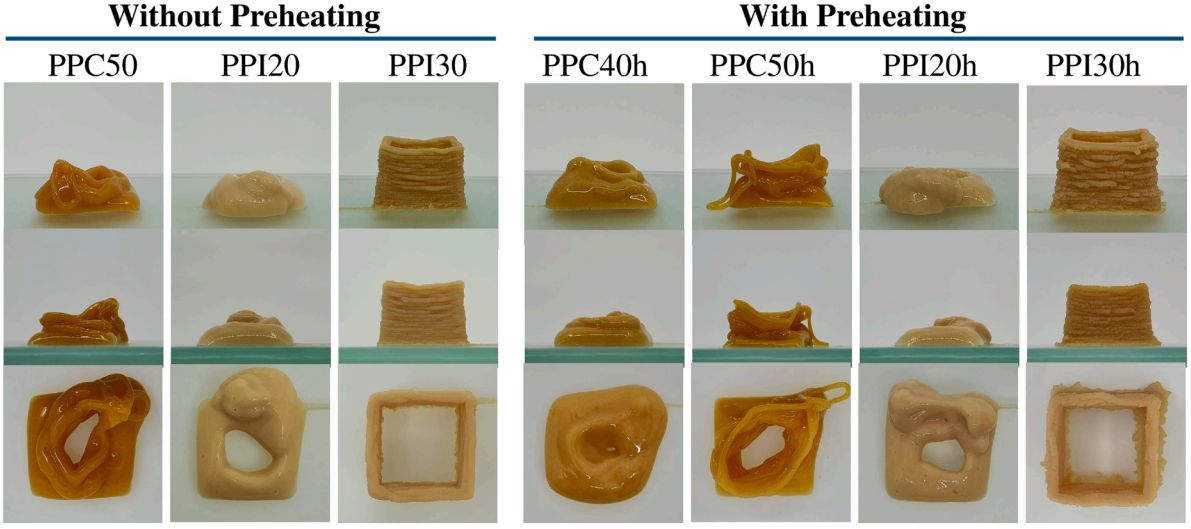

Fig. 2. Effect of concentration on 3D printed square: The 3D printed square of pea protein isolate at concentrations of 20 and 30 wt.% (PPI20 and PPI30, respectively) and pea protein concentrate at 40 and 50 wt.% (PPC40 and PPC50, respectively) from different angles without and with (indicated with an h) preheating at 60°C. PPC40 without preheating was not printable, and is therefore not shown.

PPI20h flows out less than PPC40h after being printed (see Fig. 2b).

An explanation for why PPC responded more to heating than PPI could be that the protein in PPI is likely to be more denatured, as it has been reported that commercial protein isolates tend to undergo harsh treatments resulting in denaturation (Burger et al., 2022), while proteins from concentrates are in a more native state (Dumoulin et al., 2021). PPC would then be more affected by the heat treatment since they would be able to undergo denaturing, while little would happen with PPI. Another explanation could be that during the wet-fractionation extraction of pea protein isolates, there is usually a loss of water-soluble

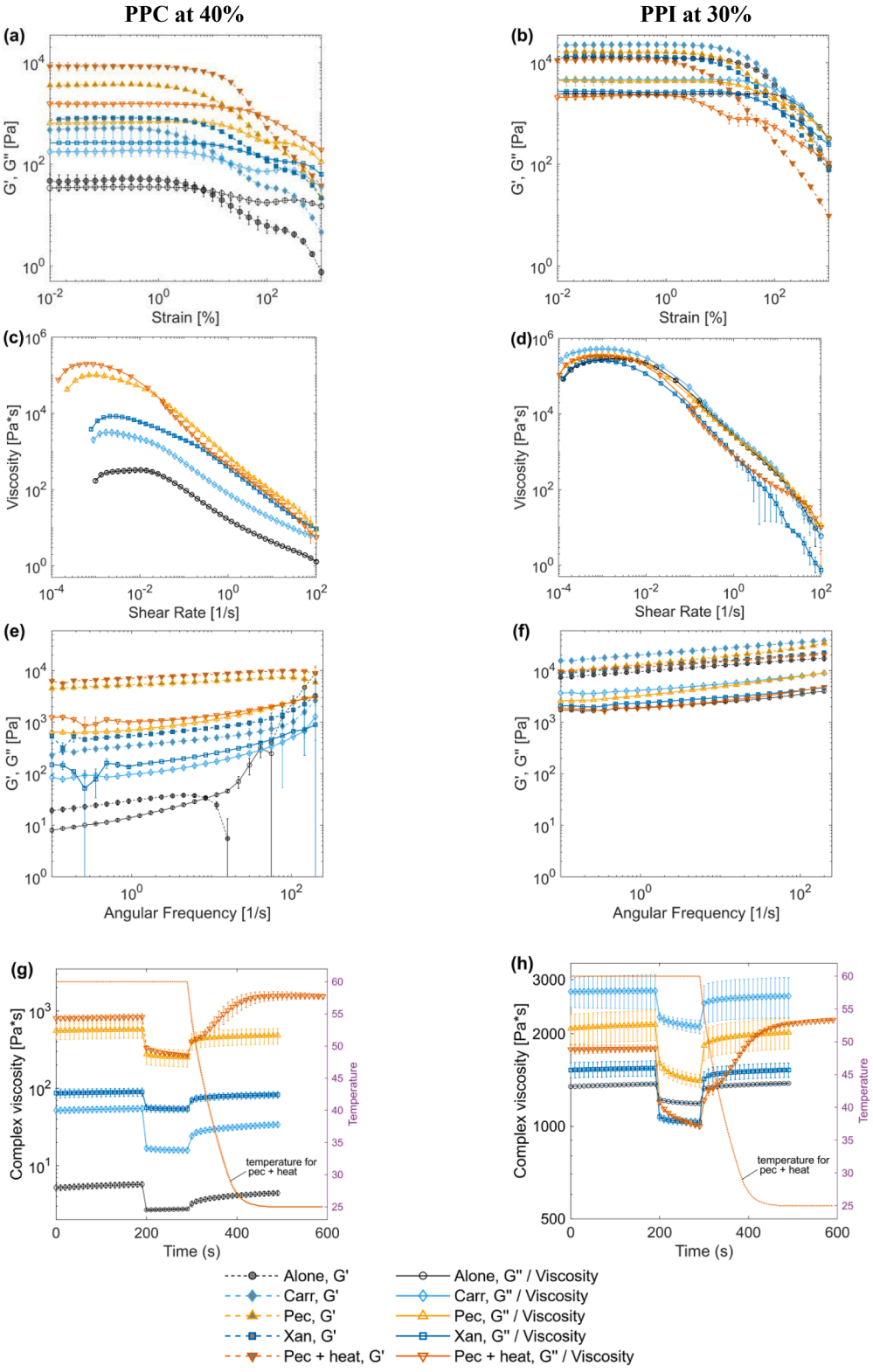

Fig. 3. Rheological properties, effect of hydrocolloid addition: (a,b) oscillatory amplitude sweep, (b,f) viscosity flow curve, (c,d) frequency sweep, and (d,h) three interval thixotropy test during low (0.05 %) and high (10 %) shear strain for (a,c,e,g) pea protein concentrate at 40 wt.%, and (b,d,f,h) pea protein isolate at 20 wt.% with pectin (Pec), carrageenan (Carr), or xanthan gum (Xan), at 1.5 wt.% For Pec + heat, the sample was heated at 60°C on the rheometer.

albumin proteins that to a larger extent consist of sulfur containing amino acids (Jiménez-Munoz et al., 2021), while the albumins would not be removed in the concentrate (Jiménez-Munoz et al., 2021). The sulfur-containing albumins in PPC can then form disulfide bonds and thereby form a more viscoelastic paste, while this would happen to a lesser extent in PPI. One last explanation is that the fibers and polysaccharides remaining in PPC could act as thickening or gelling agents during the heating, leading to a thicker paste.

Overall, the behavior of PPC and PPI as 3D printing inks was remarkably different. At the tested concentrations, PPC generally exhibited poor printability, while PPI at 30 wt.% demonstrated promising printability and retained its intended shape with good buildability, although PPI at 20 wt.% struggled to support itself adequately. Heat treatment notably enhanced the rheological properties of PPC, but it still fell short in terms of printability, with PPC50h showing limited self-supportability. For PPI30, preheating only had a slight effect on the printing resolution, resulting in minor issues such as line hanging and breaking. To further explore the printability improvements for PPI and PPC, three hydrocolloids (pectin, xanthan gum, and carrageenan) were tested in combination with PPI at 30 wt.% and PPC at 40 wt.%.

3.2. Effect of hydrocolloids

3.2.1. Rheological properties

As seen in the amplitude sweep in Fig. 3a, the addition of pectin to PPC40 resulted in a larger increase in G' and G" compared to xanthan gum and carrageenan. This trend was also seen in the flow points where PPC40Pec had a significantly higher flow point of about 0.60 kPa compared to PPC40Xan and PPC40Carr with flow points of around 0.15 and 0.03 Pa, respectively (see Table B.1 in supplementary B). Comparatively, the G' and G" of the PPI samples as well as their flow points, between 2.01 to 5.55 kPa, were still substantially and significantly higher than all PPC samples (Fig. 1b). This indicates that PPC would not have as good layer supportability as PPI even with the addition of hydrocolloids at the tested concentration. The heating of PPI30Pec on the rheometer resulted in a decrease, although insignificant, in flow point from 2.8 to 1.4 kPa while the decrease in flow point of PPC40Pec was slight (from 0.60 to 0.52 kPa). As the flow point has been suggested to indicate the force necessary to extrude the material (Liu et al., 2018; Maldonado-Rosas et al., 2022; Venkatachalam et al., 2023), the decrease in flow point of PPI would mean that a smaller force would be needed to extrude PPI when applying heat. Furthermore, the heating of PPC40Pec at 60°C on the rheometer resulted in increased G' and G", reaching close to PPI30PecH.

All samples containing hydrocolloids showed shear-thinning behavior, in the same way as pure PPI and PPC samples (Fig. 3c and Fig. 3d). Out of the PPI samples with hydrocolloids, xanthan gum resulted in the steepest slope in the viscosity flow curve, indicating stronger shear-thinning behavior and PPI30Xan also had a lower viscosity than PPI30. It has previously been seen that the addition of xanthan gum at lower concentrations than what was used in this study can increase the viscosity and improve the stability of the 3D printed object (Liu et al., 2023; Pan et al., 2022), but a too high concentration might have achieve this effect, which is supported by the findings of Liu et al. (2023). The addition of pectin and xanthan gum to PPC at 40 % increased its zero shear viscosity which was expected since these are used as thickening agents (Coultate, 2016). However, carrageenan did not increase the viscosity of PPC40 but increased the viscosity of PPI30. The addition of pectin to PPC40 increased the viscosity by about 250 times that of PPC40, which indicates that pectin can be an effective thickener used for PPC. The heating of PPC40Pec resulted in a significant further, increase of the zero shear viscosity from 69 to 130 kPa·s (see Table B.1 supplementary B), while it did not affect the zero shear viscosity of PPI30Pec remarkably. This follows the trend of PPC being more heat affected than PPI.

In the frequency sweep, all samples had gel-like behavior as there were no crossovers between G' and G" (Fig. 3e and Fig. 3f). However, for PPC40Xan, PPC40Carr and PPC40Pec, G' and G" had a stronger dependency and more pronounced slopes at higher frequency, indicating that they had softer gel-like structure. PPC40Pec had a larger gap between G' and G", indicating higher viscoelasticity. For the PPI samples, G' and G" were relatively unaffected by the frequency, indicating stable gel-like behavior. Adding carrageenan to PPI increased G' and G" in the frequency sweep, indicating a stronger gel formation. The heating of both PPI30Pec and PPC40Pec increased their viscoelasticity. Kim et al. (2021) has previously shown that their banana-pea protein printing ink with the lowest supportability in 3D printing had a G' between 2 to 10 kPa for frequencies between 0.1 and 100 rad/s (Kim et al., 2021). This can be compared to PPC40Carr and PPC40Xan, which had G' ranging from 0.2 to 1 kPa and 0.5 to 1.7 kPa, respectively which is substantially lower and would, based on their frequency sweep, likely have a poor printability. Meanwhile, PPC40Pec had G' around 4.6 to 7.3 kPa for 0.1 to 100 rad/s, which is closer to what Kim et al. (2021) had for their printing inks and might be suitable for printing. The PPI samples had comparatively much higher G', PPI30Carr ranging between 16 to 36 kPa, PPI30Xan 9 to 20.5 kPa, and PPI30Pec had 10 to 28 kPa in the frequency range of 0.1 to 100 rad/s. It has previously been suggested that a stable 3D printed object can be linked to a higher flow point, and to a higher G' (Chen et al., 2022; Liu et al., 2018). Based on that, all PPC40 samples with added hydrocolloids are expected to have better printability than PPC40 alone.

In the 3ITT (Fig. 3g and Fig. 3h), the addition of xanthan gum to PPI30 resulted in a quicker recovery from the higher shear rate. Xanthan gum has junction zones that can be easily and reversely broken (Coultate, 2016) which makes it prone to shear thinning, which might explain why the two mixtures containing xanthan gum recovered quickly in the 3ITT.

Neither PPC40Pec nor PPC40Carr recovered quickly after the high-strain period, while PPC40Xan recovered slightly quicker. For the samples heated on the rheometer, PPC40PecH and PPI30PecH, the complex viscosity increased in the 3ITT after the high strain period, during the cooling phase, although the complex viscosity increased more for PPC40PecH than PPI30PecH (see Fig. 3h). This indicates that PPC40Pec has a stronger gelling capacity than PPI30Pec.

All in all, pectin had the strongest impact on the rheological properties of the pea proteins, particularly in PPC formulations. In PPC40Pec, it is possible that pectin reinforces the paste since pectin likely can interact with pea protein (Zhang et al., 2022). Pectin significantly increased G' and G" and the flow point of PPC40, enhancing its viscoelasticity and gel-like structure more effectively than xanthan gum or carrageenan. Heating further strengthened PPC40Pec's properties, nearly matching those of PPI30PecH. In PPI formulations, carrageenan increased the gel strength, while xanthan gum intensified shear-thinning behavior and improved recovery from high shear. This suggests that hydrocolloids, particularly pectin, improve PPC's printability and supportability, although PPI remains superior in buildability and structural stability.

3.2.2. Tack-adhesion test

The tack-adhesion test offers valuable insights into the interlayer bonding potential of printed formulations, which is a critical determinant of 3D printing success in food systems. The peak force observed during separation reflects the maximum adhesive strength, while the distance at separation can indicate the extent of adhesive stretchability or ductility before failure (Kim et al., 2021). In this study, PPC40 alone exhibited minimal adhesion, pointing to its insufficient surface stickiness and/or surface hydration under the testing conditions. Interestingly, all hydrocolloids significantly enhanced the peak force required to separate PPC-based samples (Fig. 4a), suggesting improved adhesive interaction, likely mediated by the formation of a viscoelastic interfacial layer that bridges the printed layers more effectively. PPC40Pec exhibited the highest adhesive force, consistent with pectin's ability to

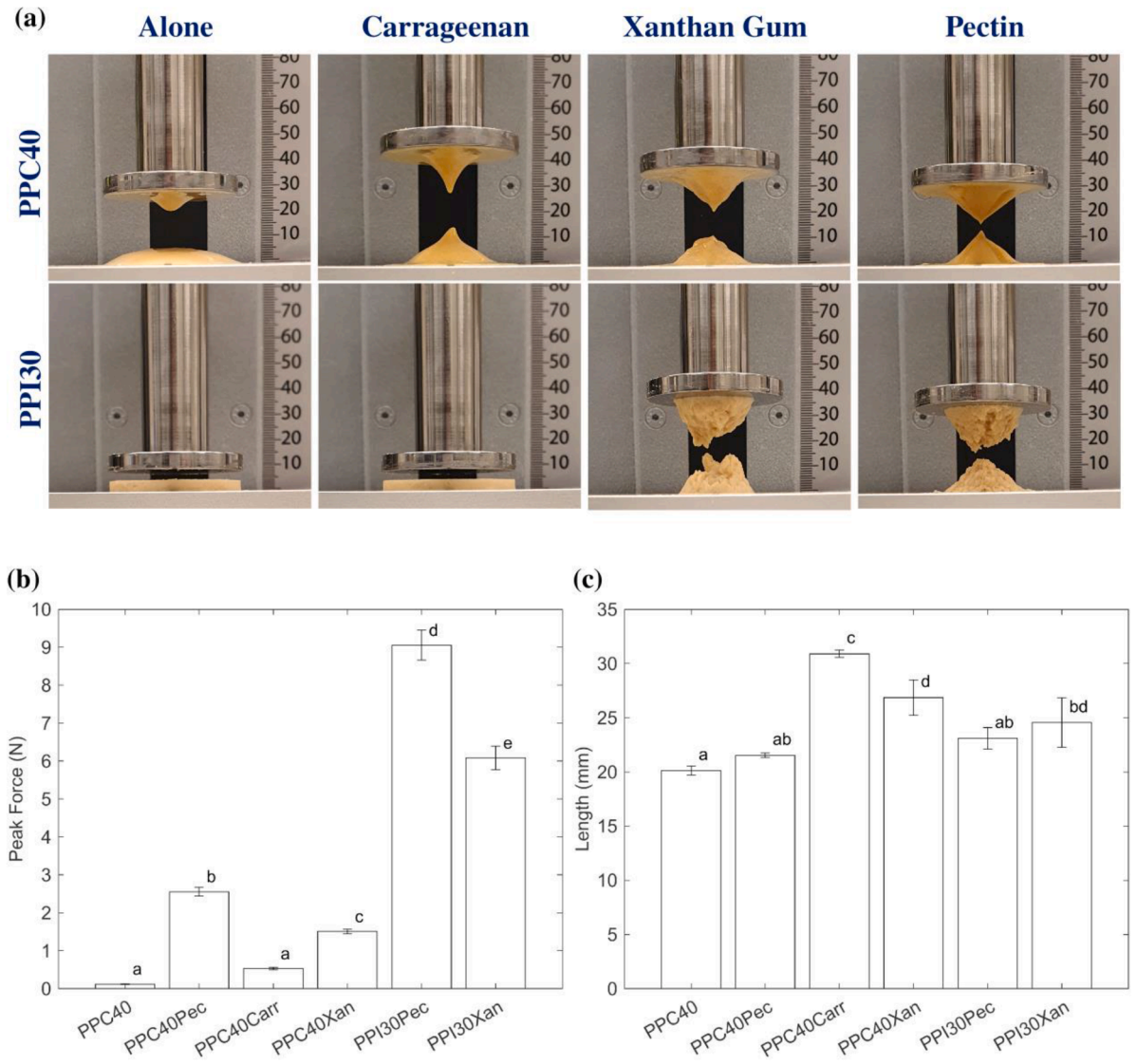

Fig. 4. Tack-adhesion test, effect of hydrocolloid addition: (a) the pictures of the separation, (b) the peak force, and (c) the length at separation of pea protein concentrate at 40 wt.% (PPC40) and pea protein isolate at 30 wt.% (PPI30) without and with 1.5 wt.% of pectin (Pec), carrageenan (Carr), and Xanthan gum (Xan) subjected to tack-adhesion test. Different letters indicate a statistical significance at α =0.05. The peak force and length at separation could not be measured for PPI30 and PPI30Carr.

form soft, sticky gels with high tackiness when interacting with proteins through hydrogen bonding and electrostatic interactions (Turgeon et al., 2007).

In contrast, PPI30 and PPI30Carr did not adhere at all during the tack test. These samples likely formed firm, elastic gel networks with high internal cohesiveness and minimal surface mobility, in line with their frequency sweep data suggesting gel-like behavior. Strong internal gelation can restrict surface flow and plasticity, both of which are essential for adhesion in layered printing contexts (Lucey & Singh, 1997). Upon addition of pectin or xanthan gum to PPI30, measurable adhesion was restored. These hydrocolloids may have disrupted the rigid protein gel matrix as seen in the CLSM micrographs of the gels (see Fig. 7), increasing surface softness and adhesiveness, as seen in other studies involving hydrocolloid-induced modulation of protein gel interfaces (Zhang et al., 2022). The higher tack force observed for PPI30Pec and PPI30Xan, coupled with their abrupt breakage behavior, suggests strong but brittle adhesive contacts, possibly due to phase-separated structures or limited energy dissipation at the interface.

These results demonstrate that the impact of pea protein fractionation method and hydrocolloids addition to them on tack-adhesion behavior is both protein- and hydrocolloid-dependent, with pectin notably enhancing adhesion in both PPC and PPI systems, although through different mechanisms, by increasing peak separation force in PPC and by reducing gel cohesiveness in PPI, enabling probe adherence. Such distinct responses underscore the importance of tailoring hydrocolloid selection based on the protein matrix to optimize layer adhesion and structural integrity in 3D printed foods

3.2.3. 3D printability as a square

The addition of xanthan gum to PPI30 resulted in a printed object with a higher resolution with clearly distinguishable, uncracked lines (see Fig. 5). However, the addition of xanthan gum to PPI30 also made the printed object softer as well as reduced the retraction response, as seen at the start and stop point in the upper right corner of the printed square from the top where there was a larger excess of printing material. Pectin also slightly improved the resolution of PPI30, while the addition of carrageenan to PPI30 resulted in lower printability in terms of resolution - it exhibited substantial cracking as well as hanging of the lines. This suggests that the more rigid gel structure carrageenan introduced in PPI may lack the flexibility needed for smooth, cohesive layer formation

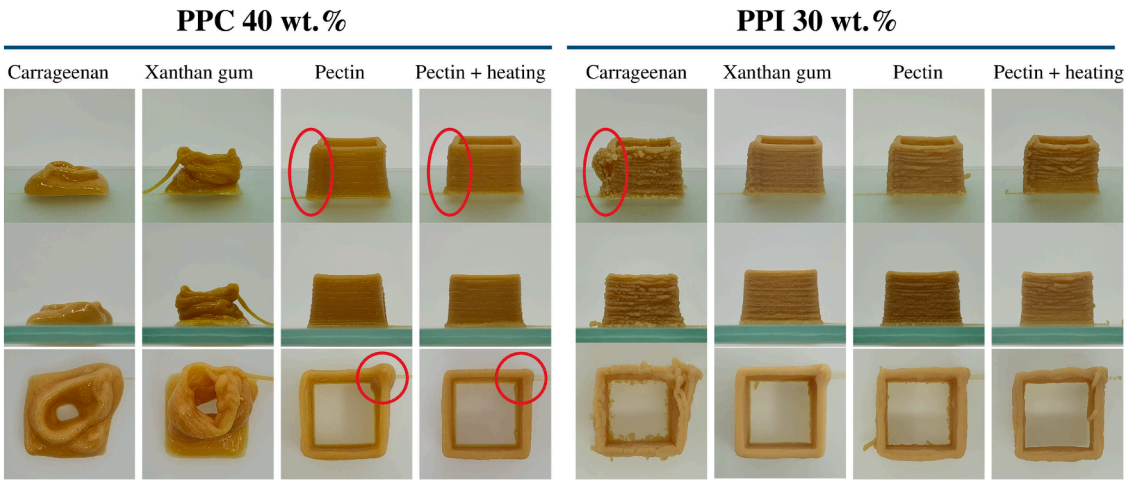

Fig. 5. 3D printed square, effect of hydrocolloids: the printed squares of pea protein isolate (PPI) at 30 wt.%, and pea protein concentrate (PPC) at 40 wt.% mixed with hydrocolloids at 1.5 wt.% without and with preheating at 60°C.

during printing.

The addition of pectin to PPC40 enabled the printing of a self-supporting and high-resolution 3D object. However, PPC40Pec did not respond to the retraction of the piston completely which resulted in an excess of material at the start and stop locations. Preheating improved the resolution of PPC40Pec while it reduced the resolution of PPI30Pec slightly. Also, PPC40PecH responded quicker to the retraction of the piston than PPC40Pec, which is seen by the reduced amount of excess material at the start and end position of the square, marked in red (see Fig. 5), indicating a reduction by the preheating at 60°C.

The addition of xanthan gum and carrageenan improved the printability of PPC slightly, but the printed objects still did not have good self-supportability. PPC40Carr had a zero shear viscosity (~2.7 kPa·s) close to the one of PPC50 (3.8 kPa·s) and they were similar in terms of printability. For future reference, a zero shear viscosity of that size could be an indicator of a too loose material for stable 3D printing. In comparison, PPC40Pec had a good printability and a zero shear viscosity of about 69 kPa·s whereas PPI30Xan, the softest of the PPI samples, had a zero shear viscosity of about 75 kPa·s. PPI30Carr had the highest zero shear viscosity of around 310 kPa·s, and it also had a poor printing resolution, indicating that this might be a too high zero shear viscosity for 3D printing at these conditions.

Connecting it to the tack-adhesion test, Kim et al. (2021) have previously speculated that the length at which the material breaks in the tack-adhesion test can be connected to the resolution of the printed object of the material, where a shorter length of break gives a higher resolution since the tailing effect is minimized when the material responds quickly to the retraction (Kim et al., 2021). PPC40Carr and PPC40Xan had the longest lengths at separation, and for PPC40Xan it is clearly visible by the trailing material that it does not respond to the piston retraction properly, and there is excess material at the start/ end position in PPC40Carr.

PPI30Carr had no adhesion to the probe, and in the square, it is possible to see that there is substantial hanging of lines, and there is a poor adhesion at the start and stop position (marked in red), resulting in a gap. It was also possible to see some hanging of lines in PPI30 without hydrocolloids. But with the addition of pectin and xanthan gum, the material could adhere to the probe, and there is substantial reduction in hanging of lines in the printing. Taken together, perhaps a too short or a non-existing break due to too high cohesiveness and lack of adhesiveness might result in the opposite issue, where the material can't adhere to the layer causing the layers to slip off. There should therefore be an optimal balance for a material where it is adhesive enough to stick to each layer, while being cohesive enough to respond quickly to the retraction of the piston and thereby avoiding tailing issues.

3.2.4. *Characterization of the printed object after post-processing*

The 3D printed cubes did not change substantially in appearance after the mild steaming. PPI30Carr had a lower printing resolution than PPI30, while PPI30Xan had a higher printing resolution than PPI30, as can be seen in Fig. 6a. PPC40Carr leaked through the metal grid and was therefore not steamed.

In the 3D printed cubes, it was also possible to see the same pattern where the heating in the cartridge appears to have improved the printability of the concentrate but not have affected the isolate much. Most of the samples had better printability when printed as a cube than as a printed square. This was probably due to the samples having more stability and support in the printed cube than in the printed square where each layer has less support. In this way, the square was a more complex object and might give a better insight into which material is the best for complex structures. However, in a meat analogue, it is likely that the structure will be more like the cube than the square.

Since PPC40Carr was not steamed, there was no texture analysis performed. The steamed object of PPI30Carr had the highest maximum force (i.e., firmness) recorded if all samples, see Fig. 6b, which is in alignment with that Cai et al. (2021) found that κ-carrageenan together with pea protein can create firm gels. Meanwhile, PPI30 containing xanthan gums had the lowest maximum forces. This suggests that xanthan gum alone would not be optimal to add to these protein samples if a firmer end-product is desired. Pectin had the opposite effect on PPI compared to PPC, where it decreased the firmness of the cubes of PPI and increased it for PPC. For PPI, both pectin and xanthan gum resulted in decreased firmness, although they improved the printing resolution, while carrageenan increased it but had a decreased resolution. This would mean that there would be a trade-off for certain hydrocolloidal additives as they might increase the resolution but then also decrease the hardness, whereas adding a hydrocolloid such as carrageenan to make it harder would reduce the printing resolution. That carrageenan increases the hardness of the steamed object is in alignment with the results of Bartkuviené et al. (2024), where the gel strength increased with carrageenan content. This is likely due to variations in protein composition and interactions in PPI and PPC. In PPI, where proteins are typically denatured and more readily form a cohesive gel (Dumoulin et al., 2021; Burger et al., 2022), the addition of pectin might disrupt the already existing protein-protein network (Yang et al., 2021), softening the overall structure and thus reducing firmness which is further supported by the CLSM micrographs (see Fig. 7). In PPC, however, which contains more native proteins and non-protein components like fibers and starch, pectin could enhance network formation by increasing cohesion among these diverse components, through for example protein-pectin interactions (Zhang et al., 2022). This leads to a denser, more rigid

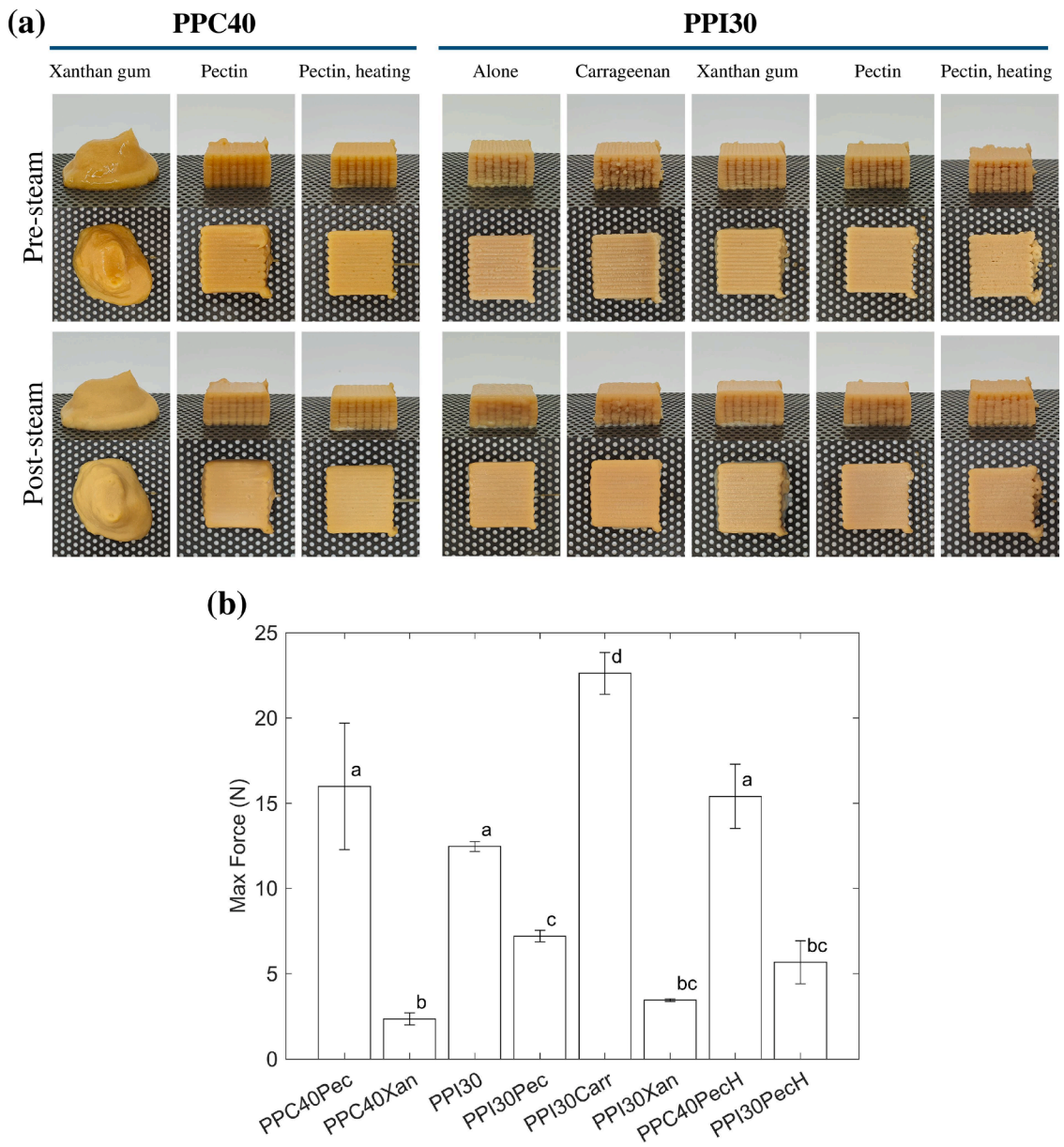

Fig. 6. Effect of hydrocolloids and post-processing on the 3D printed cube: (a) The 3D printed cube before and after a steaming treatment, (b) the maximum force at 30% single-cycle tensile compression of the post-processed cube, for pea protein isolate at 30 wt.% (PPI30), and pea protein concentrate at 40 wt.% (PPC40), mixed with the hydrocolloids carrageenan (Carr), xanthan gum (Xan), or pectin (Pec). The samples that were preheated in the cartridge at 60°C are indicated with an H. Different letters indicate a statistical significance at $\alpha = 0.05$.

structure, which accounts for the increased firmness in PPC cubes. Consequently, pectin's effect appears to depend on the composition and the protein state of each matrix, highlighting its role in either softening or strengthening gel structures.

The differing effects of pectin, xanthan gum, and carrageenan on the maximum force of PPI could be explained by their molecular structures and specific interactions with pea proteins. It has been suggested that pectin, and xanthan gum interact with proteins through hydrogen-, electrostatic-, and hydrophobic interactions (He et al., 2021; D. Zhang et al., 2022; Xie et al., 2024; Liu et al., 2023). The incorporation of pectin in pea protein isolate gels has previously been shown to improve the stability of the gels (Zhang et al., 2022). That the incorporation of pectin in PPI resulted in a less firm gel is unexpected, although this could either be attributed to that a too high hydrocolloid content was used, inducing a microphase separation and formation of a two-phase nonhomogeneous structure as shown in the CLSM micrographs (see Fig. 7). For example, He et al. (2021) found that in ginkgo seed protein-pectin gels, high methoxyl pectin had a larger decrease in gel strength at higher concentrations compared to low methoxylated pectin. The pectin used in this study was high methoxyl pectin, which means that it typically forms a stronger gel in a solution high in sugar and low in pH (Yang et al., 2022). Likely, none of those conditions were present in the PPI samples, which might explain the lack of gelation. Furthermore, preheating had no significant effect on the maximum force in the compression test. For xanthan gum, Liu et al. (2023) have previously seen that a high concentration of xanthan gum can lead to a reduced gel strength. They suggested that a two-phase system was forming at high concentrations of xanthan gum with resulting protein globules due to the repulsive forces between the negatively charged xanthan gum and proteins at pH 7 (Liu et al., 2023). This might explain the decrease in max force of the PPI30Xan gel and would mean that the concentration of each polysaccharide as well as pH would need to be optimized to get the

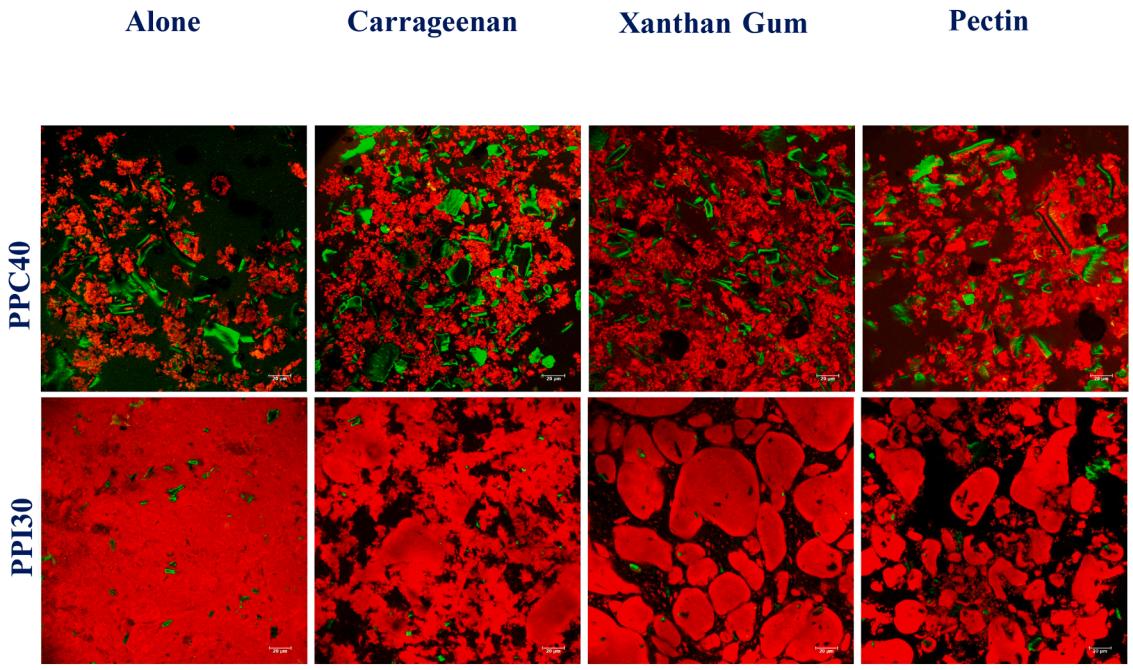

Fig. 7. Microstructure of gels, effect of hydrocolloids: the microstructure of gels with pea protein concentrate at 40 wt.% (PPC40) and pea protein isolate at 30 wt.% (PPI30) and in the presence of carrageenan, xanthan gum, and pectin at 1.5 wt.%. The red regions are proteins, and the green regions are fibers. Scalebars 20 μm.

desired consistency. Furthermore, it is possible that the different hydrocolloids could complement each other, for example, using carrageenan to gain stability and xanthan gum to improve the resolution of the printed object. It should also be noted that xanthan gum primarily acts as a thickener and rheology modifier rather than as an independent gelling agent. Future studies could therefore explore combinations of xanthan gum with gelling hydrocolloids, such as carrageenan or pectin, to simultaneously optimize printability and the texture of the final printed products.

3.2.5. *Microstructure of gels*

The microstructure visualized by the CLSM analysis of the gels can be seen in Fig. 7. In PPI30, the protein formed a dense structure. The bright red area represents the protein network, green shows fibers, whereas the black area reflects the serum phase that lacks protein. In the PPI30 sample containing carrageenan, the proteins formed a continuous phase, and carrageenan probably also formed a gel structure, resulting in a biphasic system where both components contribute to stabilize the structure, but PPI remained as the dominant continuous gel network. Cai et al. (2021), found that κ-carrageenan and pea protein form strong gels and suggested that this was due to interactions between the hydrophobic parts of protein aggregates and the carrageenan. This would reinforce the gel, and could explain why the addition of carrageenan to PPI resulted in the hardest post-steamed object. In the PPI samples with xanthan gum and pectin, the proteins formed globular domains that did not form any network. Instead, the polysaccharide phases formed the continuous phase, providing support in the structure. Since primarily xanthan gum, but also to some extent pectin gels, can flow easily upon applying stress (Coultate, 2016; Kjøniksen et al., 2005; Morris, 2019) and form weak gels, this could potentially explain the rheological properties of the printing ink of PPI30Xan and PPI30Pec as well as the increased tack, which showed a strong shear thinning behavior and a low firmness. Similar microstructure with micro-phase separation, resulting in a less homogeneous network and reduced gel hardness has been previously reported with the content of polysaccharides in protein systems such as soy and whey exceeds a specific threshold (Qiao et al., 2024; Qiao et al., 2025; van den Berg et al., 2009) which is in line with a relatively high concentration of hydrocolloids added in this study.

The microstructure of all the PPC40 gels appeared very similar, showing a protein network, although the higher fiber content in the protein concentrate disrupted the protein network, which could explain their weaker rheological properties. Also, the proteins in the network appear grainier than in the PPI30 samples, where the protein phases were smoother. These micrographs further support that fiber residues likely disrupted the protein network formation in the PPC samples since the protein is not seen to have a coherent structure as in PPI. Although the CLSM micrographs of pectin- and xanthan gum-containing PPC samples appeared similar, the marked difference in gel firmness suggests differences at the molecular interaction level. Pectin could have reinforced the protein network through electrostatic interactions and network crosslinking as previously described by Zhang et al. (2022), while xanthan gum perhaps primarily acted as a weak gel, not contributing to gelation or structural strength (Liu et al., 2023). All in all, the CLSM micrographs indicate that the main contributor to the stability of the PPI gels is the protein network and confirm that the addition of pectin and xanthan gum disrupted the protein network formation, forming a weaker structure and resulting in a weaker post-steamed printing object. This is also very much in alignment with the findings of Liu et al. (2023), where xanthan gum formed a two-phase system.

3.2.6. *Water distribution*

In TD-NMR, the T_2 relaxation time corresponds to the degree of mobility of protons where a long relaxation time means a high hydrogen mobility (Xia et al., 2024, Nasrollahzadeh et al., 2022). This can therefore be used to analyze the water distribution in food items (Chen et al., 2010). The two dominant proton populations of PPI and PPC were T_{21} (~6-82 ms) which represents water immobilized in gel network (Nasrollahzadeh et al., 2022) and T_{22} (~80-260 ms) which represents the more loosely bound or free water (Xia et al., 2024) (Fig. 8). PPC, which had the weaker steamed printed objects and therefore can be assumed to have weaker gels, had relatively larger T_{22} populations compared to PPI, which had looser bound water. However, the relaxation time of T_{21} for all PPC samples was lower than that of PPI, which could be attributed to the starch and fiber residues in PPC, which could entrap and immobilize water (Nasrollahzadeh et al., 2023). The addition of hydrocolloids had minor effect on water distribution for PPC. Pectin

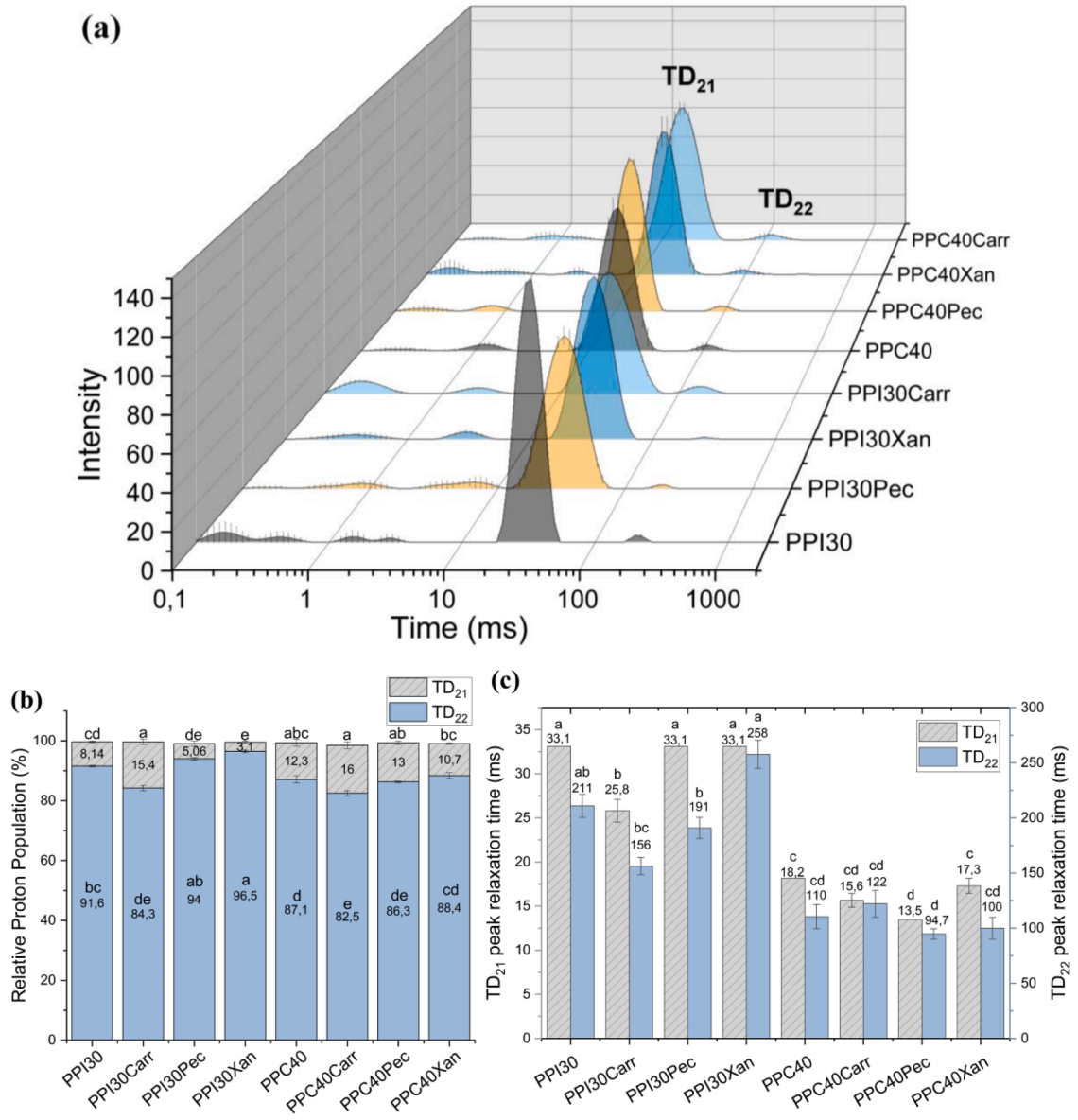

Fig. 8. Water distribution, effect of hydrocolloids: (a) the transvers relaxation time (T_2) distribution, (b) the relative proton population in the peaks, and (c) the peak relaxation times of the gels made from pea protein concentrate at 40 wt.% (PPC40) and pea protein isolate at 30 wt.% (PPI30) in the presence of carrageenan, xanthan gum, and pectin at 1.5 wt.%. No normalization to the water content has been done. Different letters indicate a statistical significance at α =0.05.

decreased the relaxation time of T_{21} for PPC significantly, suggesting that pectin contributed to further immobilizing water in the gel. The addition of the three hydrocolloids to PPI caused broadening of the T_{21} peak, showing more heterogeneity in the water populations and enhancing water immobilization. This could show that water molecules are experiencing a wider range of microenvironments due to new interactions or more complex gel microstructures formed by the combination of protein and the polysaccharide which is in line with the CLSM image of the PPI in the presence of the polysaccharides with dual or mixed networks compared to PPI alone. It has previously been reported that addition of polysaccharides to protein matrices enhances hydrogen bonding between proteins and restricts the mobility of water molecules (Liu et al., 2018; Wang et al., 2023). PPI30 with carrageenan had the firmest steamed printed object, and the broadest T_{21} proton population distribution, again in line with its very heterogeneous but protein network dominant microstructure, providing better water entrapment and texture firmness. However, it seems like neither the relative proton population nor the relaxation time can be used as sole indicators of the firmness of the gel. Rather, the strength of the gels might be attributed to the molecular properties of the proteins and hydrocolloids. This is further seen in PPI30Xan, which stood for the weakest steamed object. The addition of xanthan gum to PPI resulted in a significantly larger population in T_{21}, which means that more water is immobilized by xanthan gum, potentially implying that xanthan gum has participated less in interaction with PPI and interacted more with water. As xanthan gum also forms weak gels, this is probably the reason why the gel strength decreases despite more immobilization of the water. This is in line with the results reported by Wang et al. (2023) where addition of xanthan gum to soy protein isolate resulted in largest area of T21 in its extrudates compared with alginate and maltodextrin.

4. Conclusions

A side-by-side comparison of PPC and PPI at concentrations ranging from 10-50 wt.% as 3D printing food materials revealed that PPI achieved adequate printability at 30 wt.%, whereas PPC was unprintable

even at 50 wt.%. Limitations in the rheological properties of PPC at 40wt. % were mitigated by the addition of pectin and preheating at 60°C which very effectively improved PPC's zero shear viscosity and printability, though they had minimal effect on the PPI. The addition of xanthan gum improved the adhesion and printing resolution of PPI at 30 wt.%, albeit with a significant reduction in uniaxial compression firmness post-steaming. In contrast, carrageenan enhanced PPI's firmness after steaming but at the cost of reduced print resolution. CLSM analysis revealed that PPI formed coherent protein networks, especially when combined with carrageenan, while the addition of xanthan gum or pectin disrupted network formation, consistent with the weaker textures of the steamed printed objects. In PPC, the inherent high fiber content disrupted protein network formation, but pectin likely supported the structure via electrostatic interactions, despite the microstructure observations being similar to xanthan gum. These microstructural observations were mirrored by LF-NMR, where PPI exhibited a narrower T_{21} peak, indicating stronger and more uniform gel matrices, but it was broadened by the hydrocolloids, particularly by carrageenan, indicating structural heterogeneity and water immobilization. In contrast, PPC samples had a lower T_{21} relaxation, immobilizing water with their fibers, where pectin addition further immobilized water. The most favorable results in terms of print resolution were achieved with PPC at 40 wt.% with pectin and preheating and PPI at 30 wt.% with xanthan gum. Effective printability was associated with samples exhibiting zero shear viscosities between 70-200 kPa·s and flow points between 500-3000 Pa, with a zero shear viscosity around 100 kPa·s appearing essential for consistent 3D printing performance. Altogether, these findings suggest that while commercial PPI is inherently better suited for food 3D printing applications and that hydrocolloids could be added to tailor its applications, PPC can be made printable with appropriate modifications, particularly at higher concentrations.

Statement of human and animal rights*

Title:

The author(s) state(s) that this research was conducted in accordance with the Helsinki Declaration as revised in 2008.

There have not been any studies conducted on human or live animals in the submitted work.

Mehdi Abdollahi

CRediT authorship contribution statement

Isabel Badager: Writing – review & editing, Writing – original draft, Visualization, Software, Methodology, Investigation, Formal analysis, Data curation. **Annika Krona:** Writing – review & editing, Investigation, Formal analysis, Data curation. **Mehdi Abdollahi:** Writing – review & editing, Supervision, Resources, Project administration, Funding acquisition, Conceptualization.

Declaration of competing interest

The authors declare that they have no known competing financial interests or personal relationships that could have appeared to influence the work reported in this paper.

Acknowledgements

We would like to acknowledge FORMAS for funding this work within the 3DMix project (grant number: 2021-02349). We would like to thank Lantmännen for the contribution of their sample. We gratefully acknowledge Elahe Sharifi, Marc Weitbrecht, and José Villacís-Chiriboga for their support during analysis.

Supplementary materials

Supplementary material associated with this article can be found, in the online version, at doi:10.1016/j.fufo.2026.101128.

Data availability

Data will be made available on request.

References

Abdollahi, M., Nieuwland, M., van Bommel, K., Pouvreau, L., Ström, A., Undeland, I., 2025. Texture engineering of aquatic protein-based products via 3D food printing. Future Foods 11, 100604. https://doi.org/10.1016/j.fufo.2025.100604.

Ainis, W.N., Feng, R., van den Berg, F.W., Ahrné, L., 2023. Comparing the rheological and 3d printing behavior of pea and soy protein isolate pastes. Innov. Food Sci. Emerg. Technol. 84, 103307. https://doi.org/10.1016/j.ifset.2023.103307.

Bartkuviené, I., Keršiene̓, M., Petrikaitė, V., Leskauskaitė, D., 2024. Modulation of pea protein isolate hydrogels by adding kappa-carrageenan: gelling properties and formation mechanism. Int. J. Food Sci. Technol. 59 (9), 6598–6610. https://doi.org/10.1111/ijfs.17413.

Boukid, F., Rosell, C.M., Castellari, M., 2021. Pea protein ingredients: a mainstream ingredient to (re) formulate innovative foods and beverages. Trends Food Sci. Technol. 110, 729–742. https://doi.org/10.1016/j.tifs.2021.02.040.

Burger, T.G., Singh, I., Mayfield, C., Baumert, J.L., Zhang, Y., 2022. Comparison of physicochemical and emulsifying properties of commercial pea protein powders. J. Sci. Food Agric. 102 (6), 2506–2514. https://doi.org/10.1002/jsfa.11592.

Cai, W., Huang, W., Chen, L., 2021. Soluble pea protein aggregates form strong gels in the presence of κ-carrageenan. ACS Food Sci. Technol. 1 (9), 1605–1614. https://doi.org/10.1021/acsfoodscitech.1c00167.

Chen, F.L., Wei, Y.M., Zhang, B., 2010. Characterization of water state and distribution in textured soybean protein using dsc and nmr. J. Food Eng. 100 (3), 522–526. https://doi.org/10.1016/j.jfoodeng.2010.04.040.

Chen, J., Sun, H., Mu, T., Blecker, C., Richel, A., Richard, G., Jacquet, N., Haubruge, E., Goffin, D., 2022. Effect of temperature on rheological, structural, and textural properties of soy protein isolate pastes for 3d food printing. J. Food Eng. 323, 110917. https://doi.org/10.1016/j.jfoodeng.2021.110917.

Coultate, T.P., 2016. Food: The chemistry of its components, 6th ed. Royal Society of Chemistry.

De Angelis, D., Opaluwa, C., Pasqualone, A., Karbstein, H.P., Summo, C., 2023. Rheological properties of dry-fractionated mung bean protein and structural, textural, and rheo-logical evaluation of meat analogues produced by high-moisture extrusion cooking. Curr. Res. Food Sci. 7, 100552. https://doi.org/10.1016/j.crfs.2023.100552.

Dumoulin, L., Jacquet, N., Malumba, P., Richel, A., Blecker, C., 2021. Dry and wet fractionation of plant proteins: how a hybrid process increases yield and impacts nutritional value of faba beans proteins. Innov. Food Sci. Emerg. Technol. 72, 102747. https://doi.org/10.1016/j.ifset.2021.102747.

He, Z., Liu, C., Zhao, J., Li, W., Wang, Y., 2021. Physicochemical properties of a ginkgo seed protein-pectin composite gel. Food Hydrocoll. 118, 106781. https://doi.org/10.1016/j.foodhyd.2021.106781.

Jiménez-Munoz, L.M., Tavares, G.M., Corredig, M., 2021. Design future foods using plant protein blends for best nutritional and technological functionality. Trends Food Sci. Technol. 113, 139–150.

Johansson, L., Badager, M.I., Krona, A., Abdollahi, M., 2025. Printability and interfacial performance of emulsion gels and bigels in multi-material dual and coaxial food 3D printing. Food Hydrocoll., 111964 https://doi.org/10.1016/j.foodhyd.2025.111964.

Joyner, H.S., 2019. Rheology of semisolid foods. Springer.

Kim, Y., Kim, H.W., Park, H.J., 2021. Effect of pea protein isolate incorporation on 3d printing performance and tailing effect of banana paste. Lwt 150, 111916. https://doi.org/10.1016/j.lwt.2021.111916.

Kjøniksen, A.-L., Hiorth, M., Nyström, B., 2005. Association under shear flow in aqueous solutions of pectin. Eur. Polym. J. 41 (4), 761–770. https://doi.org/10.1016/j.eurpolymj.2004.11.006.

Lie-Piang, A., Yang, J., Schutyser, M., Nikiforidis, C., Boom, R., 2023. Mild fractionation for more sustainable food ingredients. Annu. Rev. Food Sci. Technol. 14 (1), 473–493. https://doi.org/10.1146/annurev-food-060721-024052.

Liu, Z., Bhandari, B., Prakash, S., Mantihal, S., Zhang, M., 2019. Linking rheology and printability of a multicomponent gel system of carrageenan-xanthan-starch in extrusion based additive manufacturing. Food Hydrocoll. 87, 413–424. https://doi.org/10.1016/j.foodhyd.2018.08.026.

Liu, Z., Chen, X., Dai, Q., Xu, D., Hu, L., Li, H., Hati, S., Chitrakar, B., Yao, L., Mo, H., 2023. Pea protein-xanthan gum interaction driving the development of 3d printed dysphagia diet. Food Hydrocoll. 139, 108497. https://doi.org/10.1016/j.foodhyd.2023.108497.

Liu, Z., Zhang, M., Bhandari, B., 2018. Effect of gums on the rheological, microstructural and extrusion printing characteristics of mashed potatoes. Int. J. Biol. Macromol. 117, 1179–1187. https://doi.org/10.1016/j.ijbiomac.2018.06.048.

Lucey, J.A., Singh, H., 1997. Formation and physical properties of acid milk gels: a review. Food res. int. 30 (7), 529–542.

Maldonado-Rosas, R., Tejada-Ortigoza, V., Cuan-Urquizo, E., Mendoza-Cachú, D., Morales-de La Pena, M., Alvarado-Orozco, J.M., Campanella, O.H., 2022. Evaluation

of rheology and printability of 3d printing nutritious food with complex formulations. Addit. Manuf. 58, 103030. https://doi.org/10.1016/j.addma.2022.103030.
Morris, E.R., 2019. Ordered conformation of xanthan in solutions and “weak gels”: single helix, double helix–or both? Food Hydrocoll. 86, 18–25. https://doi.org/10.1016/j.foodhyd.2017.11.036.
Nasrollahzadeh, F., Roman, L., Skov, K., Jakobsen, L.M., Trinh, B.M., Tsochatzis, E.D., Mekonnen, T., Corredig, M., Dutcher, J.R., Martinez, M.M., 2023. A comparative investigation of seed storage protein fractions: the synergistic impact of molecular properties and composition on anisotropic structuring. Food Hydrocoll. 137, 108400. https://doi.org/10.1016/j.foodhyd.2022.108400.
Nasrollahzadeh, F., Roman, L., Swaraj, V.S., Ragavan, K., Vidal, N.P., Dutcher, J.R., Martinez, M.M., 2022. Hemp (cannabis sativa l.) protein concentrates from wet and dry industrial fractionation: molecular properties, nutritional composition, and anisotropic structuring. Food Hydrocoll. 131, 107755. https://doi.org/10.1016/j.foodhyd.2022.107755.
Osswald, T., Rudolph, N., 2015. Polymer rheology. Carl Hanser, München.
Outrequin, T.C.R., Gamonpilas, C., Siriwatwechakul, W., Sreearunothai, P., 2023. Extrusionbased 3d printing of food biopolymers: A highlight on the important rheological parameters to reach printability. J. Food Eng. 342, 111371. https://doi.org/10.1016/j.jfoodeng.2022.111371.
Pan, H., Pei, F., Ma, G., Ma, N., Zhong, L., Zhao, L., Hu, Q., 2022. 3d printing properties of flammulina velutipes polysaccharide-soy protein complex hydrogels. J. Food Eng. 334, 111170. https://doi.org/10.1016/j.jfoodeng.2022.111170.
Pelgrom, P.J., Vissers, A.M., Boom, R.M., Schutyser, M.A., 2013. Dry fractionation for production of functional pea protein concentrates. Food res. int. 53 (1), 232–239. https://doi.org/10.1016/j.foodres.2013.05.004.
Provencher, S.W., 1982. A constrained regularization method for inverting data represented by linear algebraic or integral equations. Comput. Phys. Commun. 27 (3), 213–227. https://doi.org/10.1016/0010-4655(82)90173-4.
Qiao, D., Zhang, Y., Lin, L., Li, K., Zhu, F., Wang, G., Xi, G., Jiang, F., Zhang, B., Xie, F., 2024. Revealing the role of λ-carrageenan on the enhancement of gel-related properties of acid-induced soy protein isolate/λ-carrageenan system. Food Hydrocoll. 150, 109608. https://doi.org/10.1016/j.foodhyd.2023.109608.
Qiao, D., Zhang, Y., Sun, F., Yoo, M., Zhao, G., Zhang, B., 2025. Enhancement mechanism of ι-carrageenan on the network structure and gel-related properties of soy protein isolate/λ-carrageenan system. Food Chem. 468, 142476. https://doi.org/10.1016/j.foodchem.2024.142476.
Sajib, M., Forghani, B., Vate, N.K., Abdollahi, M., 2023. Combined effects of isolation temperature and ph on functionality and beany flavor of pea protein isolates for meat analogue applications. Food Chem. 412, 135585. https://doi.org/10.1016/j.foodchem.2023.135585.
Schutyser, M., Pelgrom, P., Van der Goot, A., Boom, R., 2015. Dry fractionation for sustainable production of functional legume protein concentrates. Trends Food Sci. Technol. 45 (2), 327–335. https://doi.org/10.1016/j.tifs.2015.04.013.
Tan, C., Toh, W.Y., Wong, G., Li, L., 2018. Extrusion-based 3d food printing–materials and machines. Int. J. Bioprinting 4 (2). https://doi.org/10.18063/IJB.v4i2.143.
Toker, O.S., Karasu, S., Yilmaz, M.T., Karaman, S., 2015. Three interval thixotropy test (3itt) in food applications: A novel technique to determine structural regeneration of mayonnaise under different shear conditions. Food Res. Int. 70, 125–133. https://doi.org/10.1016/j.foodres.2015.02.002.
Turgeon, S.L., Schmitt, C., Sanchez, C., 2007. Protein-polysaccharide complexes and coacervates. Current Opin. Coll. Interf. Sci. 12 (4–5), 166–178. https://doi.org/10.1016/j.cocis.2007.07.007.
Van den Berg, L., Rosenberg, Y., Van Boekel, M.A., Rosenberg, M., Van de Velde, F., 2009. Microstructural features of composite whey protein/polysaccharide gels characterized at different length scales. Food Hydrocoll. 23 (5), 1288–1298.
Venkatachalam, A., Balasubramaniam, A., Wilms, P.F., Zhang, L., Schutyser, M.A., 2023. Impact of varying macronutrient composition on the printability of pea-based inks in extrusion-based 3d food printing. Food Hydrocoll. 142, 108760. https://doi.org/10.1016/j.foodhyd.2023.108760.
Wang, F., Gao, Y., Gu, X., Luan, B., Zhu, Y., Huang, Y., Zhu, X., 2023. High-moisture extrusion cooking on soybean-wheat protein mixtures: effect of sodium alginate/xanthan gum/maltodextrin on promoting a fibrous structure. Front. nutr. 9, 1077601. https://doi.org/10.3389/fnut.2022.1077601.
Wen, Y., Chao, C., Che, Q.T., Kim, H.W., Park, H.J., 2022. Development of plant-based meat analogs using 3d printing: status and opportunities. Trends Food Sci. Technol. https://doi.org/10.1016/j.tifs.2022.12.010.
Wilms, P., Daffner, K., Kern, C., Gras, S., Schutyser, M., Kohlus, R., 2021. Formulation engineering of food systems for 3d-printing applications–a review. Food Res. Int. 148, 110585. https://doi.org/10.1016/j.foodres.2021.110585.
Xia, W., Czaja, T.P., Via, M., Zhang, H., Clausen, M.P., Ahrné, L., 2024. Acid-induced gels from mixtures of micellar casein and pea protein: effect of protein ratio and preheating route. Food Hydrocoll. 153, 110045. https://doi.org/10.1016/j.foodhyd.2024.110045.
Xie, J., Bi, J., Jacquet, N., Blecker, C., Feng, S., Liu, X., Lyu, J., 2024. Structure formation mechanism of pectin-soy protein isolate gels: unraveling the role of peach pectin fractions. Int. J. Biol. Macromol. 281, 136429. https://doi.org/10.1016/j.ijbiomac.2024.136429.
Yang, X., Li, A., Li, D., Guo, Y., Sun, L., 2021. Applications of mixed polysaccharideprotein systems in fabricating multi-structures of binary food gels—a review. Trends Food Sci. Technol. 109, 197–210. https://doi.org/10.1016/j.tifs.2021.01.002.
Yang, X., Yuan, K., Descallar, F.B.A., Li, A., Yang, X., Yang, H., 2022. Gelation behaviors of some special plant-sourced pectins: A review inspired by examples from traditional gel foods in china. Trends Food Sci. Technol. 126, 26–40. https://doi.org/10.1016/j.tifs.2022.06.012.
Zhang, D., Chen, D., Patel, B., Campanella, O.H., 2022. Pectin as a natural agent for reinforcement of pea protein gel. Carbohydr. Polym. 298, 120038. https://doi.org/10.1016/j.carbpol.2022.120038.
Zhang, M., Vora, A., Han, W., Wojtecki, R.J., Maune, H., Le, A.B., Thompson, L.E., McClelland, G.M., Ribet, F., Engler, A.C., et al., 2015. Dual-responsive hydrogels for direct-write 3d printing. Macromolecules 48 (18), 6482–6488. https://doi.org/10.1021/acs.macromol.5b01550.